Korean J. Chem. Eng., 34(5), 1500-1503 (2017)
DOI: 10.1007/s11814-017-0034-0

pISSN: 0256-1115
eISSN: 1975-7220

Photodegradation of organic dyes via competitive direct reduction/indirect oxidation on $InSnS_2$ under visible light

Sungmook Park, Woocheol Kim, and Younghun Kim†

Department of Chemical Engineering, Kwangwoon University, Wolgye-dong, Nowon-gu, Seoul 01899, Korea
(*Received 25 December 2016 • accepted 6 February 2017*)

Abstract−A visible-light-responsive photocatalyst, SnS_2, was prepared by a rapid microwave-assisted method. This photocatalyst showed a narrow band gap (~2.0 eV) and a broad-spectrum response in the range of 400-800 nm. To enhance its photocatalytic activity, the surface of SnS_2 was modified with indium-doping and loading of a noble metal. The photocatalytic activity of SnS_2, $InSnS_2$, and Pt/$InSnS_2$ was evaluated by photodegradation of methyl orange (MO) and rhodamine B (RhB) under visible light. While direct reduction via a photoelectron was the major reaction in the degradation of MO, indirect oxidation (deethylation) via reactive oxygen species (·OH and $\cdot O_2^-$) in the degradation of RhB was accompanied subsequently with direct reduction (cycloreversion). Therefore, photocatalytic efficiency and the mechanism for photodegradation of organic dyes depended on the types of organic dyes.

Keywords: Photocatalyst, Microwave-assisted, SnS_2, Organic Dyes, Visible-light-responsive

INTRODUCTION

Semiconductor photocatalysts have been widely used in green chemistry technology, such as water purification and hydrogen production [1-3]. The main advantage of photocatalysis is that complete mineralization or degradation to CO_2, H_2O, and small moieties of a wide range of pollutants can potentially be achieved at room temperature. TiO_2 photocatalyst has been most frequently employed for the elimination of organic pollutants in wastewater due to its low cost, high stability, and non-toxicity [4]. However, TiO_2 has a well-known limitation: the wide band gap (3.2 eV) limits its operating conditions, i.e., working under UV irradiation. Thus, metal sulfides (CdS, SnS_2, etc.) are becoming a promising family of visible-light-responsive photocatalysts owing to their narrow band gap energy (2.0-2.3 eV) [5]. The n-type semiconductor SnS_2, in particular, has good stability in acid and neutral aqueous solutions against oxidation and photocorrosion, compared to CdS [6].

SnS_2 nanostructures have been successfully prepared by a hydrothermal process using autoclave or microwave. The microwave-assisted method is suitable to prepare nanostructured SnS_2 under mild conditions with shorter times and lower temperatures than a common autoclave-assisted method [7]. To improve photocatalytic efficiency, a few studies have tried to modify the band structure by doping foreign elements (Ce^{3+}, Zn^{2+}, and In^{3+}) on SnS_2 [8]. Lei and co-workers reported that the flowerlike In^{3+}-doped SnS_2 as photocatalyst was successfully prepared by a hydrothermal method [9]. However, the system was driven by UV light, and SnS_2 was prepared by a conventional heating process at high temperatures and with long heating times.

Herein, a flower-like In^{3+}-doped SnS_2 ($InSnS_2$) was prepared by a facile and rapid microwave-assisted method under mild conditions without templates or surfactants, and was applied to photocatalytic degradation of organic dyes under LED visible-light. In addition, platinum dot employed as an electron trap was immobilized on the surface of $InSnS_2$ to enhance the activity of the individual photocatalyst via separation of electrons and holes.

EXPERIMENTAL

The typical synthetic process for $InSnS_2$ was followed as described in our previous report [6,8]. The mixture of 1 mM $SnCl_4$, 10 mM thioacetamide, and 0.05 M $InCl_3$ was transferred into a 100 mL Teflon vessel. Briefly, the microwave-heating method we used can be described as: 100 °C for 1 h in a microwave reaction system (MARS6, CEM) at 1,800 W and 2,455 MHz of magnetron frequency. The reaction products, orange-colored particles, were washed three times with water and ethanol. 1 wt% of Pt dots was loaded on $InSnS_2$ particle by reduction of K_2PtCl_6 using $NaBH_4$ [8]. Finally, SnS_2, $InSnS_2$, and Pt/$InSnS_2$ were dried at 80 °C in a drying oven for 24 h.

Photocatalytic activities of SnS_2, $InSnS_2$, and Pt/$InSnS_2$ were evaluated by the photodegradation of methyl orange (MO, $C_{14}H_{14}N_3NaO_3S$) containing a N=N double bond and rhodamine B (RhB, $C_{28}H_{31}ClN_2O_3$) without a N=N double bond, under visible-light irradiation at room temperature. A low-powered white-LED lamp with 48 W (UHP-LED-White, Prizmatix) was used as the light source. The photocatalytic tests were performed with 0.1 g of photocatalysts suspended in 10 ppm of MO and 5 ppm of RhB aqueous solution. The suspension was stirred in the dark for 1 h to ensure the adsorption/desorption equilibrium. The concentration of MO and RhB in aqueous solution was determined by UV-vis spectroscopy (UV-1800, Shimadzu).

The crystalline structure and morphology of samples were analyzed by X-ray diffraction (XRD, SC222, PANalytical) and scan-

†To whom correspondence should be addressed.
E-mail: korea1@kw.ac.kr

ning electron microscopy (SEM, TESCAN VEGA3, Tescan). Band-gap energy was calculated by spectrum data analyzed with UV-vis diffusion reflectance spectroscopy (UV-DRS, V-670, JASCO).

RESULT AND DISCUSSION

SnS_2 and $InSnS_2$ were prepared by a facile microwave-assisted method, which required a short heating time and mild temperature/pressure conditions, compared to a common hydrothermal method and solid-state reaction [10]. Since the crystallinity of photocatalysts was a crucial factor in photocatalytic activity, crystalline structure and band gap energy was first analyzed with XRD and UV-vis DRS, respectively. Even though the microwave-assisted method required milder conditions than hydrothermal method, as-made SnS_2 showed well-crystallized without other impurities, as shown in Fig. S1. The diffraction peaks of SnS_2 can be indexed to the standard hexagonal phase of SnS_2 (JCPDS #23-677), and no peaks from impurities of $InSnS_2$ indicated that indium was incorporated into the SnS_2 lattice without destruction of the hexagonal phase structure. A similar mechanism to Ag^+ doped into a SnS_2 lattice was reported [11], and a certain amount of Sn^{4+} ions was substituted with Ag^+ without destruction of the phase structure. Therefore, there was no peak change or addition in XRD patterns.

The capacities for visible-light absorption and crystallinity are also important to photocatalytic performance and were analyzed with UV-vis DRS (Fig. S2(a)). SnS_2 and $InSnS_2$ samples exhibited broad-spectrum responses in the range of 400-800 nm, indicating that the samples were excellent visible-light-responsive photocatalysts for degradation of organic dyes. The band gap energy based on Tauc's formula [12] was calculated as 2.02 and 2.0 eV for SnS_2 and $InSnS_2$ (Fig. S2(b)), and the deposition of Pt dots on SnS_2 did not change the band gap (2.0 eV) of $InSnS_2$ [8]. As compared with the band gap of bulk SnS_2 (~2.18 eV) and TiO_2 (~3.2 eV), a red shift of SnS_2 samples prepared here gives suitable properties to be activated by visible light for photocatalytic degradation of organic dyes. The morphology of SnS_2 and $InSnS_2$ was investigated using SEM (Fig. S3) and showed a flower-like structure, which was open porous structures for more efficient transportation of reactants into the active sites to enhance the photocatalytic efficiency.

The photocatalytic activities of SnS_2, $InSnS_2$, and $Pt/InSnS_2$ were evaluated by photodegradation of MO and RhB under visible light irradiation. Since MO has N=N double bond and RhB does not, the photodegradation mechanism of MO might be different with that of RhB. Both Sn(II) and Sn(IV) compounds in SnS_2 samples are known to exist, and reducible cation (tetravalent) and oxidizable cation (divalent) are generally associated with electron and hole conduction, respectively [13]. Thus, two paths for the photocatalytic degradation of organic dyes correlated with the existence of reduction by electron conduction and oxidation by hole conduction. As shown in Fig. 1(a) and Fig. S4, the photocatalytic degradation of MO under visible-light was dependent on exposure time. The characteristic absorbance peak at 465 nm of MO without blue-shift of peak gradually decreased within 2 h, namely, the main peak of MO showed hypochromic shift without hypsochromic shift. The mineralization ratio (r=VC/m) for effective degradation of organic dyes by photocatalysts was calculated with experimental conditions, where, V, C, and m are volume (250 mL) and concentration (10 mg/L) of MO, and mass (100 mg) of SnS_2, respectively. The ratio of SnS_2 showed 0.025, and appears higher compared to literature data: 0.016 for SnS_2 nanoflower [14], 0.005 for SnS_x/TiO_2 composite [15], and 0.02 for SnS_2 nanoparticle [16]. The variation of normalized concentration (C/C_o) of MO in the presence of different photocatalysts was plotted in Fig. 1(b). The order of photodegradation activity of MO over three samples follows $InSnS_2$>Pt/$InSnS_2$>SnS_2. The apparent rate constants (k, 10^2 min^{-1}) calculated by pseudo-first-order kinetics are 3.19, 2.12, and 1.69 for $InSnS_2$, $Pt/InSnS_2$, and SnS_2, respectively. While indium doping on SnS_2 enhanced the photodegradation of MO, the deposition of noble metal (Pt dots) was not increased by photocatalytic activity. It might be due to the difference of photodegradation mechanisms such as direct reduction of electron and indirect oxidation of oxidized radicals (·OH and $\cdot O_2^-$). By indium doping on SnS_2, photocatalytic performance for Cr(VI) reduction [8] and degradation of organic dyes [9] was enhanced compared pure SnS_2.

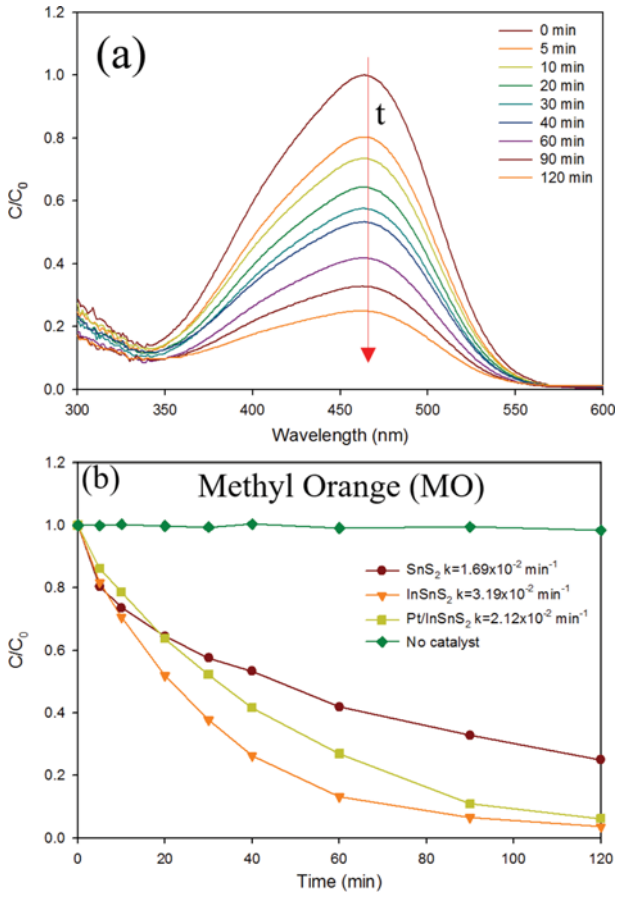

Fig. 1. (a) Time dependent UV-vis absorption spectrum of MO (C_o= 10 mg/L) in the presence of SnS_2, and (b) variation of normalized concentration (C/C_o) of MO with irradiation time under visible-light conditions.

This feature could be found the photodegradation of RhB in Fig. 2. While the photocatalytic degradation of RhB by using SnS_2 was completed within 2 h (Fig. 2(a)), that of $InSnS_2$ and $Pt/InSnS_2$ was finished within 1 h (Fig. 2(b)). Both indium doping and depo-

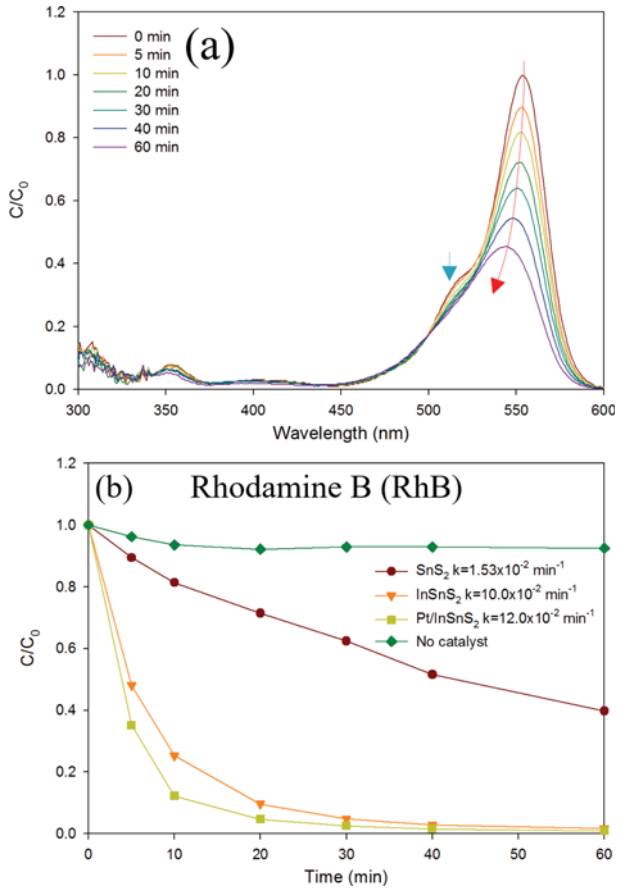

Fig. 2. (a) Time dependent UV-vis absorption spectrum of RhB (C_o= 5 mg/L) in the presence of SnS_2, and (b) variation of normalized concentration (C/C_o) of RhB with irradiation time under visible-light conditions.

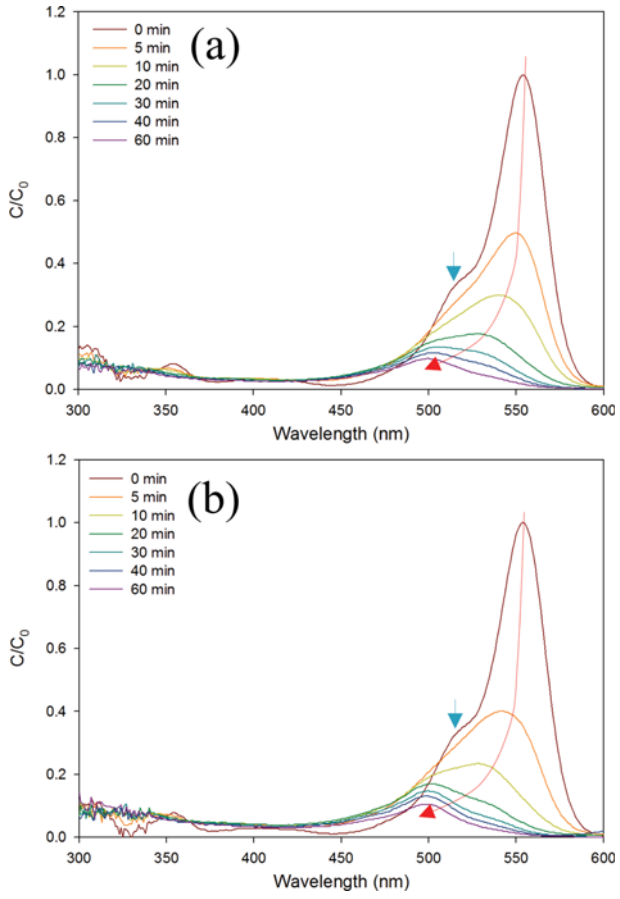

Fig. 3. Time dependent UV-vis absorption spectrum of RhB (C_o=10 mg/L) in the presence of (a) $InSnS_2$ and (b) $Pt/InSnS_2$ under visible-light conditions.

sition of noble metal might enhance the photocatalytic degradation of RhB. If the absorption intensity of RhB at 554 nm continuously decreased without a blue-shift in UV-vis spectrum (only hypochromic shift), there would be decomposition mechanism involving cleavage of the whole conjugated chromophore structure (cycloreversion) [17], i.e., the absence of the aromatic moieties [18]. As shown in Fig. 3, the absorption peak at 554 nm in UV-vis spectrum of photodegradation of RhB using $InSnS_2$ and $Pt/InSnS_2$ also showed a blue-shift with continuously decreased. Therefore, this hypsochromic and hypochromic shift of the absorbance maximum has been proven to be derived from step-by-step deethylation of RhB to give *N*-de-ethylated intermediates [18]. The apparent rate constants (k) calculated of $Pt/InSnS_2$, $InSnS_2$, and SnS_2 are 12.0, 10.0, and 1.53, respectively. In this case, the deposition of noble metal positively influenced on the photodegradation of RhB. Therefore, the main degradation mechanism for MO differs from RhB.

The photodegradation of organic dyes followed the direct reduction via electron and indirect oxidation via oxidized radicals (·OH and $\cdot O_2^-$). As shown in Fig. 4(a), photo-reduction of MO was worked with photoelectrons via Sn^{IV}/Sn^{II} transition and subsequent oxidation was activated with ·OH and $\cdot O_2^-$ radicals [5,6]. Pt dots in $InSnS_2$ acted as an effective inhibitor of electron-hole recombination, and thus Pt adsorbed the photogenerated electron to form reactive oxygen species, which indirectly used to photooxidize MO. Since no blue-shift in degradation of MO was found in UV-vis spectrum, direct reduction (cleavage of the whole chromophore) of N=N double bond was major reaction compared to indirect oxidation (deethylation). Whereas, Pt dots in $InSnS_2$ for photodegradation of RhB effectively formed the reactive oxygen radicals, which used to deethylation of RhB. Finally, photodegradation rate of $Pt/InSnS_2$ compared to $InSnS_2$ was enhanced. Therefore, in degradation of RhB, indirect oxidation was a major reaction, and direct reduction of cycloreversion was a subsequent reaction.

CONCLUSIONS

Visible-light derived photocatalyst (SnS_2) was prepared by a rapid microwave-assisted method and the surface structure of SnS_2 was modified with indium doping and Pt-loading to enhance the photocatalytic activity. To confirm enhancement of photoactivity of $InSnS_2$ and $Pt/InSnS_2$, organic dyes (MO w/ and RhB w/o N=N double bond) was photodegraded under a white-LED lamp. For MO degradation, direct reduction of N=N bonds via photoelectron was the major photodegradation mechanism (hypochromic without hypsochromic shift in UV-vis spectrum). In the case of

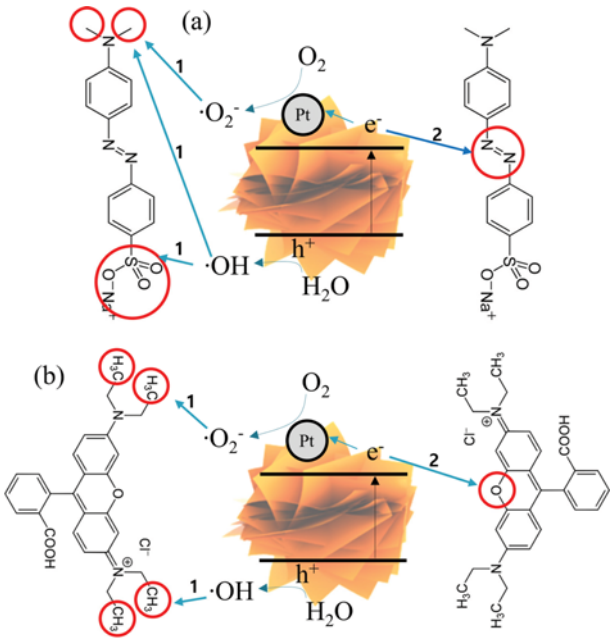

Fig. 4. Photodegradation mechanisms of (a) MO and (b) RhB through (1) indirect oxidation and (2) direct reduction.

RhB, indirect oxidation (deethylation) via reactive oxygen species was major (hypochromic and hypsochromic shift in UV-vis spectrum) and cycloreversion was the subsequent reaction. Therefore, although the surface modification using indium doping and Pt deposition was effectively enhanced its photocatalytic activity, the degradation mechanisms were different with target organic dyes.

ACKNOWLEDGEMENTS

This work was supported by the Research Grant of Kwangwoon University (2017) and the Korea Environmental Industry and Technology Institute (201400-0140002).

SUPPORTING INFORMATION

Additional information as noted in the text. This information is available via the Internet at http://www.springer.com/chemistry/journal/11814.

REFERENCES

1. J. Romao and G. Mul, *ACS Catal.*, **6**, 1254 (2016).
2. A. Umar, M. S. Akhtar, A. Al-Hajry, M. S. Al-Assiri, G. N. Dar and M. S. Islam, *Chem. Eng. J.*, **262**, 588 (2015).
3. X. Wang, M. Hong, F. Zhang, Z. Zhuang and Y. Yu, *ACS Sustainable Chem. Eng.*, **4**, 4055 (2016).
4. C. Lalhriatpuia, A. Tiwari, A. Shukla, D. Tiwari and S. M. Lee, *Korean J. Chem. Eng.*, **33**, 3367 (2016).
5. X. Li, J. Zhu and H. Li, *Appl. Catal. B: Environ.*, **123-124**, 174 (2012).
6. S. Park, J. Park, R. Selvaraj and Y. Kim, *J. Ind. Eng. Chem.*, **31**, 269 (2015).
7. J. Park, S. Park, R. Selvaraj and Y. Kim, *RSC Adv.*, **5**, 52737 (2015).
8. S. Park, R. Selvaraj, M. A. Meetani and Y. Kim, *J. Ind. Eng. Chem.*, **45**, 206 (2017).
9. Y. Lei, S. Song, W. Fan, Y. Xing and H. Zhang, *J. Phys. Chem. C*, **113**, 1280 (2009).
10. G. Kiruthigaa, C. Manoharan, C. Raju and S. Dhanapandian, *Mater. Sic. Semicond. Process.*, **26**, 533 (2014).
11. X. Zhang, W. Xu, Z. Xie and Y. Wang, *J. Mater. Chem. A*, **4**, 1908 (2016).
12. Y. C. Zhang, Z. N. Du, S. Y. Li and M. Zhang, *Appl. Catal. B: Environ.*, **95**, 153 (2010).
13. A. A. Burton, D. Colombara, R. D. Abellon, F. C. Grozema, L. M. Peter, T. J. Savenije, G. Dennler and A. Walsh, *Chem. Mater.*, **25**, 4908 (2013).
14. H. Liu, Y. Su, R. Chen and Y. Wang, *J. Mol. Catal. A: Chem.*, **378**, 285 (2013).
15. C. Yang, W. Wang, Z. Shan and F. Huang, *J. Solid State. Chem.*, **182**, 807 (2009).
16. Y. C. Zhang, Z. N. Du, J. W. Li and M. Zhang, *Sep. Purif. Technol.*, **81**, 101 (2011).
17. A. Akhundi and A. Habibi-Yangjeh, *Mater. Chem. Phys.*, **174**, 59 (2016).
18. Y. Lu, Y. Zhao, J. Zhao, Y. Song, Z. Huang, F. Gao, N. Li and Y. Li, *Cryst. Growth Des.*, **15**, 1031 (2015).

Supporting Information

Photodegradation of organic dyes via competitive direct reduction/indirect oxidation on $InSnS_2$ under visible light

Sungmook Park, Woocheol Kim, and Younghun Kim†

Department of Chemical Engineering, Kwangwoon University, Wolgye-dong, Nowon-gu, Seoul 01899, Korea
(*Received 25 December 2016 • accepted 6 February 2017*)

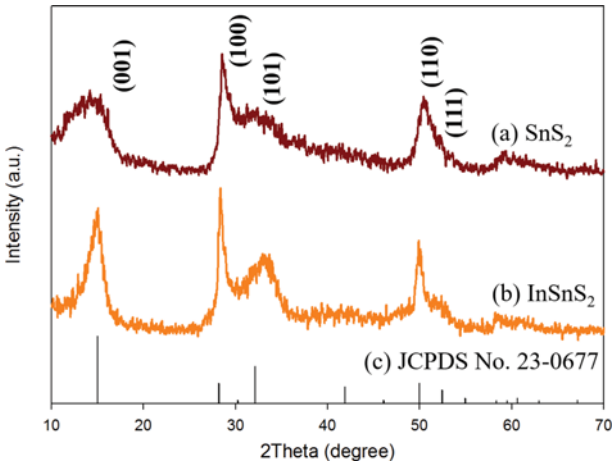

Fig. S1. XRD patterns of (a) SnS_2 and (b) $InSnS_2$ samples prepared using microwave method. Peaks in (c) represent corresponding positions of standard hexagonal phase SnS_2.

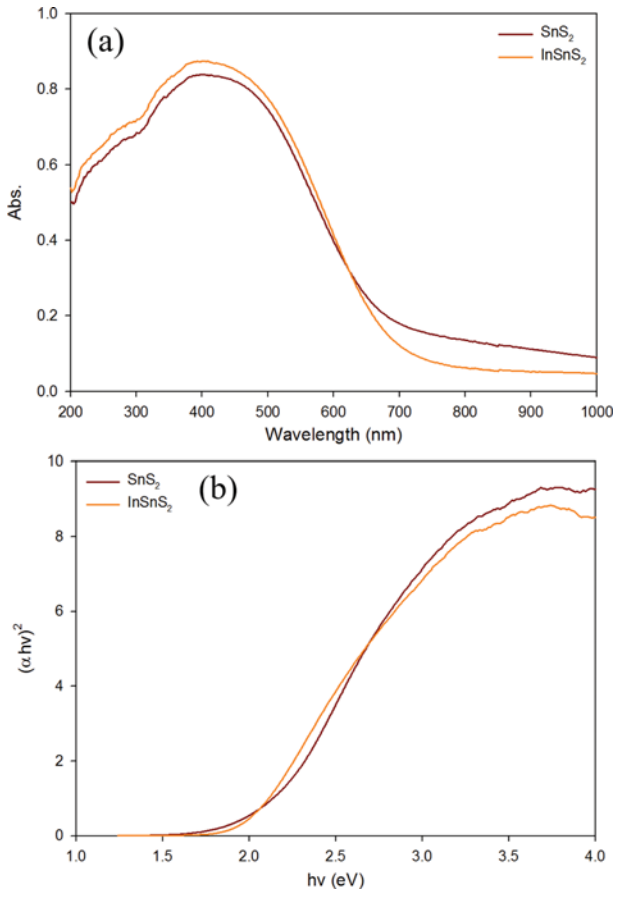

Fig. S2. (a) UV-vis DRS spectra and (b) band gap energies estimated by $(\alpha h\nu)^2$ versus the photo-energy ($h\nu$) of SnS_2 and $InSnS_2$ samples.

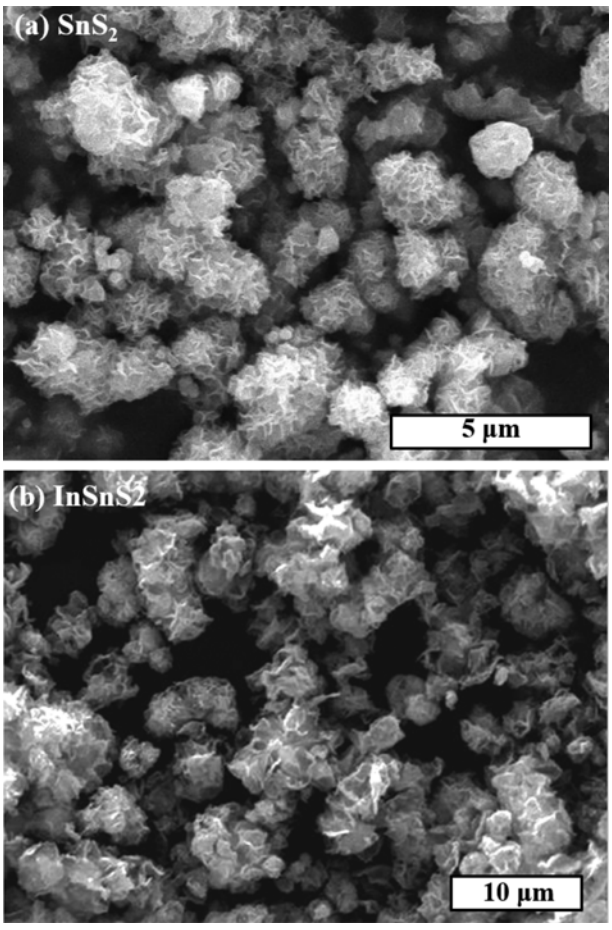

Fig. S3. SEM images of (a) SnS_2 and (b) $InSnS_2$ samples.

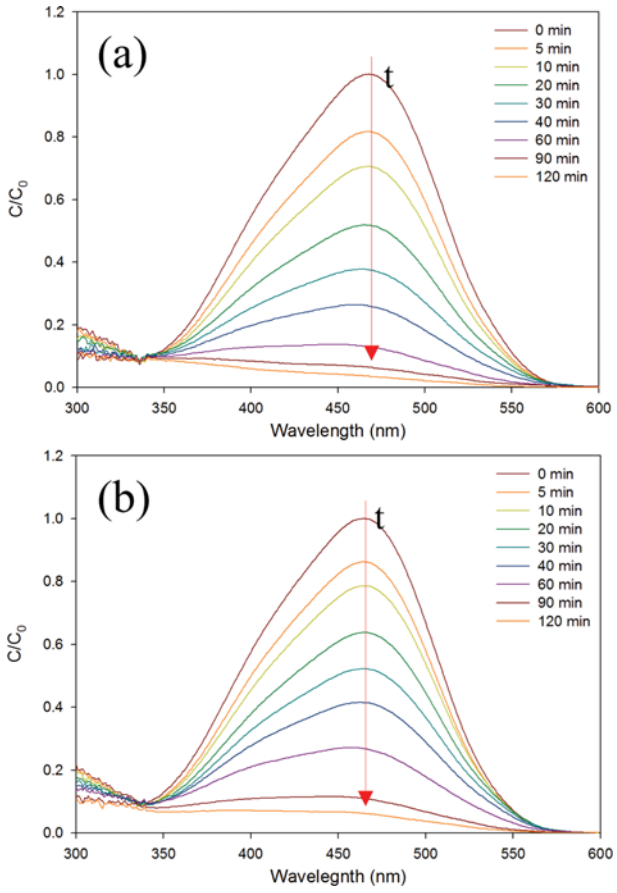

Fig. S4. Time dependent UV-vis absorption spectrum of MO (C_o= 10 mg/L) in the presence of (a) $InSnS_2$ and (b) Pt/$InSnS_2$ under visible-light conditin.